Dyes and Pigments 95 (2012) 732–742

Contents lists available at SciVerse ScienceDirect

Dyes and Pigments

journal homepage: www.elsevier.com/locate/dyepig

Access to a large stokes shift in functionalized fused coumarin derivatives by increasing the geometry relaxation upon photoexcitation: An experimental and theoretical study

Dandan Huang, Yinghui Chen, Jianzhang Zhao*

State Key Laboratory of Fine Chemicals, School of Chemical Engineering, Dalian University of Technology, E-208 West Campus, 2 Ling-Gong Road, Dalian 116024, PR China

ARTICLE INFO

Article history:
Received 28 March 2012
Received in revised form
22 April 2012
Accepted 23 April 2012
Available online 17 May 2012

Keywords:
Coumarin
Density functional theory
Geometry relaxation
Photochemistry
Photophysics
Stokes shift

ABSTRACT

A series of new fluorophores with a fused coumarin framework were prepared. The dyes show red-shifted and enhanced absorption compared to the model compound, 7-hydroxycoumarin. The new coumarin bearing a 4-dimethylaminophenylacetylide group, shows absorption at 389 nm (ε = 14,300 M^{-1} cm^{-1}), compared to the model compound which shows blue shifted absorption bands (ε = 11,500 M^{-1} cm^{-1} at 320 nm). The emission of the new coumarin bearing a 4-dimethylaminophenylacetylide group is remarkably red-shifted (λ_{em} = 555 nm) compared to the model compound (λ_{em} = 356 nm). The fluorescence quantum yields of the new coumarins are increased up to ca. 9-fold compared to the model compound. The Stokes shifts (84 nm–166 nm) are also much larger than that of the model compound. TDDFT calculations show that the fused coumarins undergo significant geometry relaxation upon photoexcitation, which is responsible for the large Stokes shift. Population of the triplet excited state was observed for the bromo-functionalized coumarin.

1. Introduction

Coumarin has been used as fluorophore in chemosensors, light-harvesting molecular arrays and photosensitizers for photovoltaics [1–6]. However, coumarin suffers from some disadvantages, such as the small Stokes shift. The typical Stokes shift for coumarin dyes is less than 30 nm [7–10]. Thus, new coumarin derivatives that show large Stokes shift are highly desired. However, the typical strategies used in the derivatization of a fluorophore, such as extension of the π-conjugation framework, is not helpful to increase the Stokes shift, although this strategy is very often effective to shift the absorption/emission to longer wavelength [10–22]. For example, acetylide substituents have been attached to the π-core of coumarin and red-shifted absorption/emission wavelength were observed, but the Stokes shift does not increase remarkably [11,12]. The failure to increase the Stokes shift with the extension of the π-conjugation of a fluorophore is not unexpected. In principle, the large Stoke shift is caused by remarkable molecular geometry relaxation upon photoexcitation (that is, the geometry relaxation after the Franck–Condon transition, as well as the geometry relaxation immediately after the vertical emission to the ground state). On the contrary, the absorption/emission wavelength of a fluorophore are mainly due to the size of the π-conjugation framework. Furthermore, the coumarin derivatives are limited to a large extent to those with large π-conjugation framework by attaching acetylide or benzothioazole moieties [11,12]. Coumarin derivatives with new molecular structures are desired to explore the photophysical properties.

In order to address the above challenges, herein we prepared new coumarin derivatives with the novel *fused coumarin* structure (**C-2** – **C-4**, Scheme 1). The most striking photophysical properties of the new dyes are the large Stokes shift compared to the unsubstituted 7-hydroxycoumarin (**C-1**). Furthermore, the new derivatives show stronger absorption in the visible range and the emission is greatly red-shifted compared to the model coumarin **C-1**. With DFT calculations, we found that the large Stokes shift of the new coumarin dyes is due to the remarkable molecular *geometry relaxation* upon photoexcitation. Our complementary experimental and theoretical work on the fused coumarins is useful for the design of new fluorophores that show predetermined photophysical properties, such as large Stokes shifts.

* Corresponding author. Tel./fax: +86 411 3960 8007.
E-mail address: zhaojzh@dlut.edu.cn (J. Zhao).

0143-7208/$ – see front matter © 2012 Elsevier Ltd. All rights reserved.
doi:10.1016/j.dyepig.2012.04.024

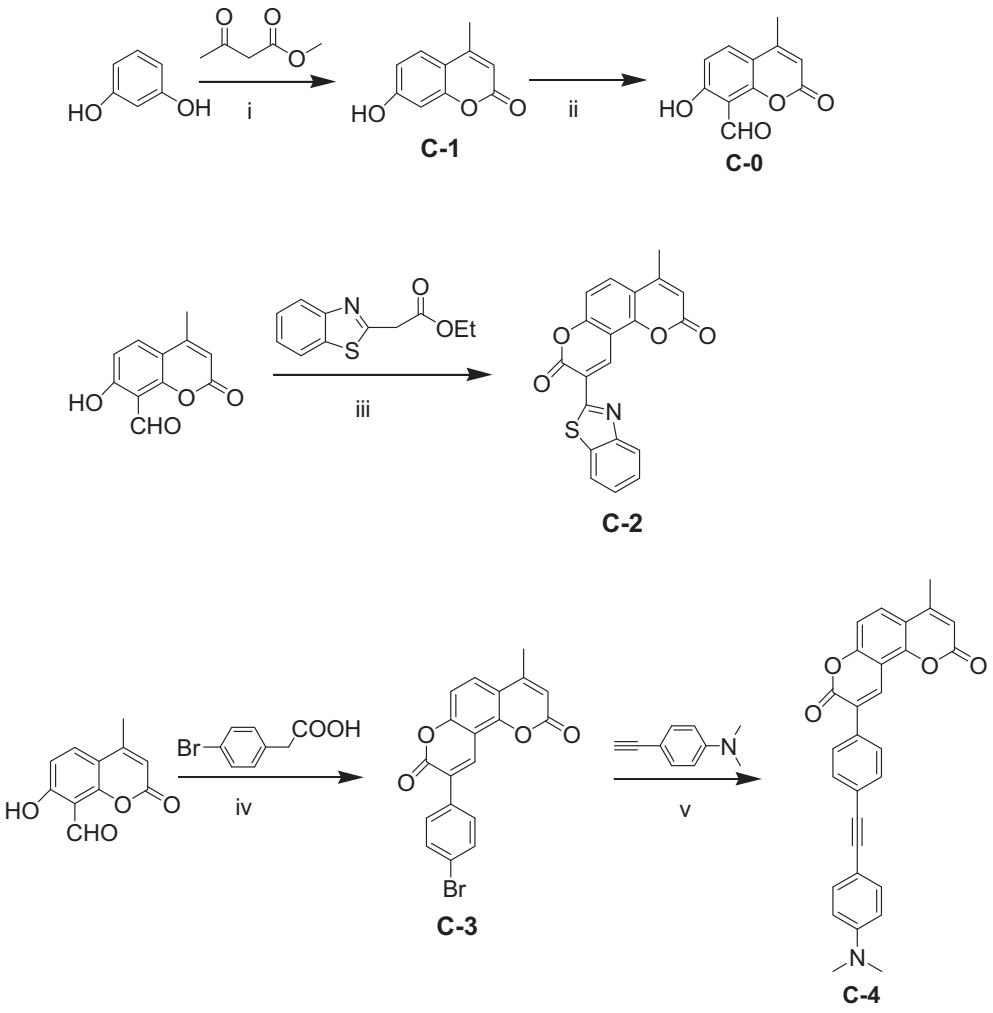

Scheme 1. Synthesis of the new coumarin derivatives: **C-1**, **C-2**, **C-3** and **C-4**. Reagents and conditions: (i) H_2SO_4, THF, reflux, 3 h, 65%. (ii) (a) CH_3COOH, hexamethylenetetramine, reflux, 7 h (b) 20% HCl, reflux, 45 min, 10%. (iii) N_2, CH_3OH, piperidine, reflux, 7 h, 75%. (iv) acetic anhydride, triethylamine, reflux, 8 h, 55%. (v) N_2, THF, triethylamine, $Pd(PPh_3)_2Cl_2$, CuI, reflux, 7 h, 63%.

2. Experimental section

2.1. General information

NMR spectra were measured on a 400 MHz Varian Unity Inova spectrophotometer. Mass spectra were recorded on Q-TOF Micro MS spectrometer. UV–Vis spectra were measured on an Agilent HP8453 UV–visible spectrophotometer. Fluorescence spectra were recorded on Shimadzu RF5301PC spectrofluorometer. Fluorescence quantum yields were measured with quinine sulfate as standard ($\Phi_F = 54.6\%$ in 0.05 M H_2SO_4). Luminescence lifetimes were measured on a OB920 fluorescence lifetime spectrometer (Edinburgh Instruments, U.K.). 8-formyl-7-hydroxy-4-methylcoumarin (compound **C-0**) was prepared according to a literature method [15].

2.2. DFT calculations

All the calculations are based on density functional theory (DFT) with B3LYP functional and 6–31G(d) basis set. Toluene was used as solvent in all the calculations (PCM model). The UV–vis absorptions (vertical excitation) were calculated with the time-dependent DFT (TDDFT) method based on the optimized ground state geometry (S_0 state). For the fluorescence, the emission wavelength was calculated based on the optimized excited states geometries (S_1 state, etc). All these calculations were performed with Gaussian 09W [13].

2.3. Synthesis

2.3.1. C-2

Under N_2 atmosphere, 8-formyl-7-hydroxy-4-methylcoumarin (102.0 mg, 0.5 mmol) was dissolved in anhydrous methanol (10 mL). 2-(2′-benzothiazolyl) acetate (110.0 mg, 0.5 mmol) and piperidine (10 μL, 0.1 mmol) were added, and the solution was heated under reflux. Precipitate appeared after 15 min. The solution was heated under reflux for 5 h. After cooling to room temperature, water (15 mL) was added and the mixture was stirred for 15 min. The precipitate was collected by filtration, the solid was washed with water and cold methanol. The crude product was dried under vacuum (144.0 mg, 75%). ^{1}H NMR (400 MHz, $CDCl_3$): 9.67 (s, 1H), 8.17 (d, 1H, $J = 8.0$ Hz), 8.03 (d, 1H, $J = 8.0$ Hz), 7.93 (d, 1H, $J = 8.0$ Hz), 7.59 (t, 1H, $J = 16.0$ Hz), 7.48 (t, 1H, $J = 16.0$ Hz), 7.43 (d, 1H, $J = 8.0$ Hz), 6.42 (s, 1H), 2.55 (s, 3H). Selected IR data (cm^{-1}, KBr pellet): $\nu = 755$, 826, 876, 1001, 1169, 1389, 1579, 1611, 1731, 1750, 3061, 3084. MALDI-HRMS: calcd ($[C_{20}H_{11}NO_4S+Na]^+$) $m/z = 384.0306$, found, $m/z = 384.0309$.

2.3.2. C-3

8-formyl-7-hydroxy-4-methylcoumarin (0.26 g, 1.96 mmol), *p*-bromobenzeneacetic acid (0.50 g, 2.32 mmol), acetic anhydride (0.90 g, 8.86 mmol), triethylamine (0.28 g, 3.77 mmol) were mixed, and the solution was heated under reflux for 8 h. Precipitate

appeared after cooling to room temperature. Water (10 mL) was added and the pH was brought to 7 with 10% NaOH aqueous solution. Precipitate was collected with filtration. The solid was washed with water (10 mL) and cold methanol (10 mL). The product was dried under vacuum (410.0 mg, 55%). ^{1}H NMR (400 MHz, $CDCl_3$): 8.44 (s, 1H), 7.76 (d, 1H, $J = 8.0$ Hz), 7.67 (d, 2H, $J = 8.0$ Hz), 7.62 (d, 2H, $J = 12$ Hz), 7.31 (d, 1H, $J = 8.0$ Hz), 6.35 (s, 1H), 2.50 (s, 3H), ^{13}C NMR (100 MHz, $CDCl_3$): 159.42, 159.11, 155.23, 152.49, 150.06, 132.92, 131.92, 131.75, 130.18, 127.54, 126.98, 123.79, 115.85, 114.07, 112.64, 109.11. Selected IR data (cm^{-1}, KBr pellet): $\nu = 778$, 819, 1084, 1168, 1388, 1578, 1621, 1732, 2921, 2967, 3084. MALDI-HRMS: calcd ($[C_{19}H_{11}{}^{79}BrO_4]^+$), $m/z = 381.9841$, found, $m/z = 381.9845$.

2.3.3. C-4

C-3 (109.0 mg, 0.287 mmol), 4-ethynyl-N,N-dimethylbenzenamine (50.0 mg, 0.345 mmol) was mixed in THF (4 mL) and triethylamine (4 mL). $Pd(PPh_3)_2Cl_2$ (5 mol %, 10.0 mg), PPh_3 (5 mol %, 4.0 mg) and CuI (5 mol %, 3.0 mg) was added to the mixture. The solution was heated under reflux for 8 h. After the reaction was complete, the solvent was evaporated under reduced pressure. The crude product was purified using column chromatography (silica gel, CH_2Cl_2) to give C-4 as brownish red powder. (49.0 mg, 63%). ^{1}H NMR (400 MHz, $CDCl_3$): 8.47 (s, 1H), 7.79 (d, 2H, $J = 8.0$ Hz), 7.75 (d, 1H, $J = 8.0$ Hz), 7.60 (d, 2H, $J = 8.0$ Hz), 7.46 (d, 2H, $J = 8.0$ Hz), 7.32 (d, 1H, $J = 8.0$ Hz), 6.71 (d, 2H, $J = 8.0$ Hz), 6.35 (s, 1H), 3.02 (s, 6H), 2.50 (s, 3H). Selected IR data (cm^{-1}, KBr pellet): $\nu = 778$, 816, 849, 1084, 1168, 1359, 1526, 1597, 1615, 1727, 2205, 2817, 2901, 3066. MALDI-HRMS: calcd ($[C_{29}H_{21}NO_4]^+$), $m/z = 447.1471$, found, $m/z = 447.1472$.

3. Results and discussion

3.1. Design and synthesis of the new coumarin derivatives

Previously coumarin derivatives were prepared by extension of the π-conjugation framework of the fluorophore [11,12], for example, with the benzothiazole moiety. Another strategy to prepare coumarin derivatives that show long absorption/emission wavelength is to use suitable polycyclic aromatic hydrocarbons as the starting material [14].

We notated that formyl-coumarin was reported [15]. Based on the synthetic method of the benzothiazole coumarin derivatives, this intermediate compound can be used to *fuse* an extra coumarin unit, thus fused coumarin **C-2** was prepared (Scheme 1). The two coumarin fluorophores in **C-2** are *integrated* together, or fused together. To the best of our knowledge, this is the first time that such a fluorophore structure is reported. In order to prove that this derivatization method can be extended to prepare more highly functionalized derivatives, **C-3** was prepared with the 2-(4-bromophenyl)acetic acid as the starting material. The bromo substitution can be used for further derivatization, which was demonstrated by the preparation of **C-4**, in which an electron-donating moiety was readily introduced to the phenyl substituents by Sonogashira coupling reaction. The new coumarin derivatives show larger Stokes shift than the model coumarin. All the photophysical properties were rationalized by DFT/TDDFT calculations.

3.2. UV–Vis absorption and fluorescence spectra of the compounds

The UV–Vis absorption of the dyes were studied (Fig. 1). All the new derivatives show a more red-shifted absorption than the model coumarin **C-1**. For example, **C-2** and **C-4** shows absorption maxima at 373 nm and 389 nm, respectively. Conversely **C-1** didn't show any absorptions in this range. However, **C-3** shows absorption similar to **C-1**, indicating that the intramolecular charge transfer (ICT) effect is also important for the absorption of the coumarin derivatives [10]. For **C-3**, we propose that the ICT character is not significant, whereas for **C-2** and **C-4**, the ICT effect is more significant.

The fluorescence excitation and emission spectra of the compounds were studied (Fig. 2). **C-1** shows emission at 356 nm, and the emission band is mainly located in the UV range. For **C-2**, the excitation is red-shifted to 373 nm, and the emission band is located at 461 nm, and almost all the emission band is located in the visible range. Similar excitation and emission bands were observed for **C-3** (Fig. 2c). For **C-4**, in which the ICT character is more remarkable compared to **C-2** and C-**3**, the emission is red-shifted to 555 nm (Fig. 2d). The emission bands of **C-2** and **C-3** show vibrational progression, which is similar to the emission of **C-1**. For **C-2**, the structureless emission band indicates a significant ICT feature of the emissive state.

Small Stokes shift (56 nm) was observed for **C-1** (Fig. 2a). For **C-2**, the Stokes shift increased to 87 nm. Similar large Stokes shift was observed for **C-3**. For **C-4**, the Stokes shift is up to 144 nm, which is ca. 3-fold of **C-1**. To the best of our knowledge, this is among the largest Stokes shifts observed for coumarin derivatives [12]. Previously coumarins with benzothiazole moiety were used for fluorescent molecular probes, but the fluorophore shows a small Stokes shift of 20 nm [9]. The coumarin derivatives with large Stokes shifts described herein, especially **C-4**, can be developed as fluorophores for fluorescent molecular probes. The large Stokes shift of fluorophore can reduce the self-absorption, or the inner filter effect and it is beneficial for fluorescence sensing [10].

We found that the emission wavelength of the derivatives can be readily tuned from 356 nm (**C-1**) to 555 nm (**C-4**). Furthermore, the fluorescence quantum yield was greatly improved. For example, the fluorescence quantum yield of **C-1** is 0.037, but **C-2** and **C-4** show fluorescence quantum yield at above 0.30 (Table 1). The variation of the emission wavelength and the emission intensity is discernable with unaided eye (Fig. 3b). With excitation by a 365 nm lamp **C-1** gives a weak blue emission, **C-2** gives strong cyan emission and notably **C-4** gives strong yellow emission. The vivid emission color and the intense emission will be beneficial for fluorescent bioimaging applications [9,16].

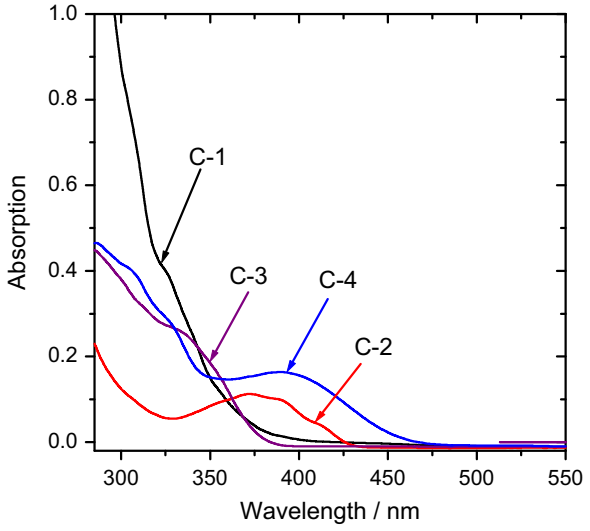

Fig. 1. UV–Vis absorption spectra of compounds **C-1**, **C-2**, **C-3** and **C-4**. $c = 1.0 \times 10^{-5}$ mol dm^{-3} in toluene. 20 °C.

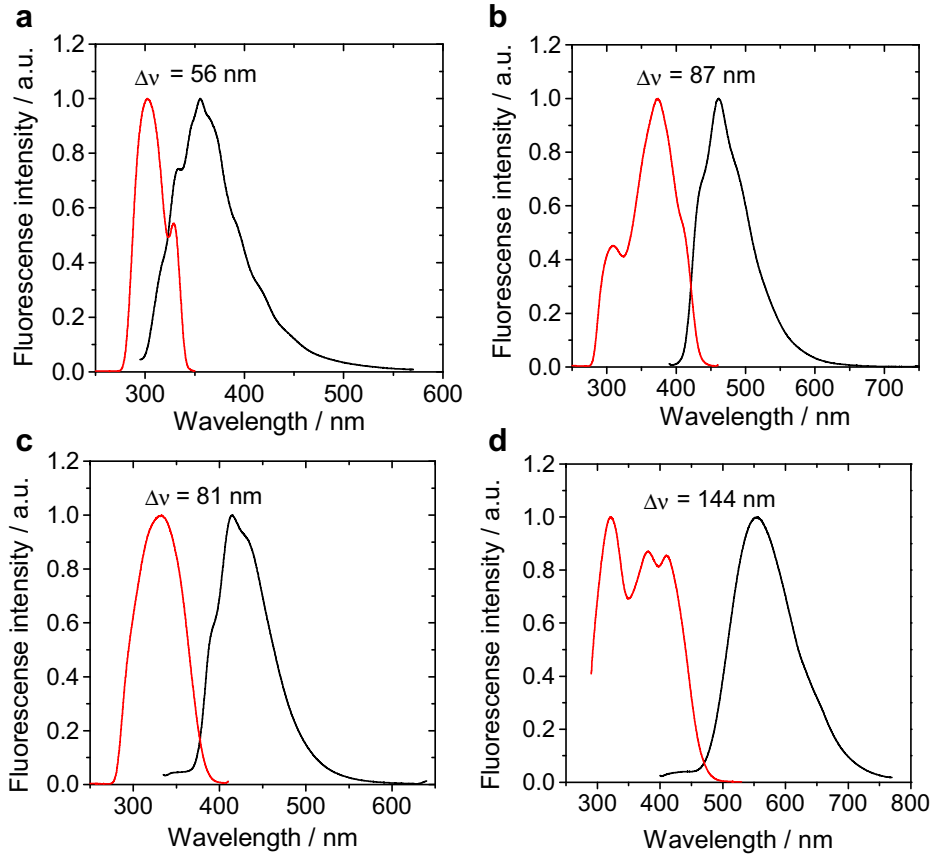

Fig. 2. Normalized emission and excitation spectra of compounds (a) **C-1**, λ_{ex} = 300 nm; (b) **C-2**, λ_{ex} = 380 nm; (c) **C-3**, λ_{ex} = 315 nm; and (d) **C-4**. λ_{ex} = 390 nm $c = 1.0 \times 10^{-5}$ mol dm^{-3} in toluene, 20 °C.

The new coumarin derivatives show enhanced luminescence property at solid state relative to the model example **C-1** (Fig. 4). **C-1** gives weak emission at solid state, whereas **C-2**, **C-3** and **C-4** give intense emission in the solid. Furthermore, we found that the emission of **C-2** is red-shifted by 87 nm relative to that in solution. **C-3** gives emission at 450 nm, which is red-shifted by 40 nm compared to that in solution. **C-4** gives emission at 587 nm, the red-shift compared to that in solution (555 nm, Fig. 2d) is not significant. The emission intensity and the emission color were demonstrated by the photographs of the luminescence in solid (Fig. 4b). **C-2** gives bright yellow emission and **C-4** gives golden emission color. Emission at solid state is interesting and can be used for electroluminescence [11].

The photophysical parameters were summarized in Table 1. The UV–Vis absorption, the emission wavelength and the fluorescence quantum yields of the dyes are improved relative to that of the model coumarin **C-1**.

3.3. Polarity sensitivity of the fluorescence

The coumarin derivatives show drastically different polarity-dependent fluorescence (Fig. 5). For example, the emission maximum of **C-1** was red-shifted with increasing the solvent polarity (Fig. 5a). The emission is centered at 356 nm in toluene, and the emission band is red-shifted to 379 nm in methanol. The emission intensity also changes significantly with changes to the solvent polarity. Interestingly, **C-2** shows similar emission wavelength in different solvents, but the emission intensity decreases slightly in highly polar solvents, such as in acetonitrile and methanol, than that in toluene or dichloromethane (Fig. 5b).

The emission of **C-3** shows similar solvent polarity-dependency relative to **C-2**. It should be noted that the solvent polarity-dependency of the emission of **C-2** and **C-3** is unusual [10,12,17]. Normally the fluorescent dyes show emission wavelength changes in solvents with different polarity, for example, the bathochromic

Table 1
Photophysical parameters of the coumarin derivatives **C-1**, **C-2**, **C-3** and **C-4**.

Sensors	ε[a] (M^{-1} cm^{-1})	λ_{abs} (nm)	λ_{em} (nm)	Stokes Shift/(nm)	Φ[b]	τ/ns	k_r[c]	k_{nr}[d]
C-1	1.15×10^4	320	356	56	0.037	2.2	1.68×10^7	4.38×10^7
C-2	9.14×10^3	373	461	87	0.320	3.5	9.14×10^7	1.94×10^7
C-3	2.04×10^4	327	410	81	0.139	1.2	1.16×10^7	7.18×10^7
C-4	1.43×10^4	389	555	144	0.323	3.2	1.01×10^7	2.11×10^7

[a] ε: Molar extinction coefficient, in toluene (1.0×10^{-5} mol dm^{-3}); λ_{abs}: Absorption wavelength (wavelength of first absorption maximum), in toluene (1.0×10^{-5} mol dm^{-3}); λ_{em}: emission wavelength (at the maximum intensity) in solution and in solid state; Stokes' shifts.
[b] Fluorescence quantum yields; τ: fluorescence lifetimes, The excitation wavelength for the fluorescence spectra equals to the maximum UV–Vis absorption wavelength.
[c] Are radiative and nonradiative transition rate constants, respectively. In s^{-1}.
[d] Are radiative and nonradiative transition rate constants, respectively. In s^{-1}.

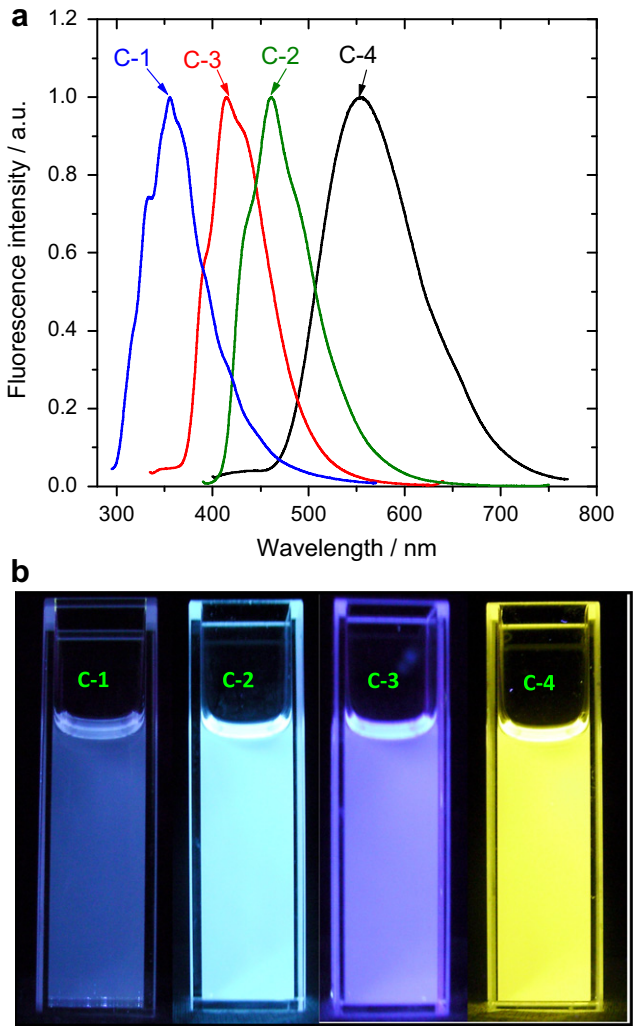

Fig. 3. (a) Normalized emission spectra of compounds **C-1**, **C-2**, **C-3**, **C-4**. λ_{ex} [**C-1**] = 300 nm, λ_{ex}[**C-2**] = 380 nm, λ_{ex} [**C-3**] = 315 nm, λ_{ex} [**C-4**] = 390 nm. (b) Fluorescence photographs of compounds **C-1**, **C-2**, **C-3** and **C-4** under UV lamp excitation (365 nm). $c = 1.0 \times 10^{-5}$ mol dm^{-3} in toluene. 20 °C.

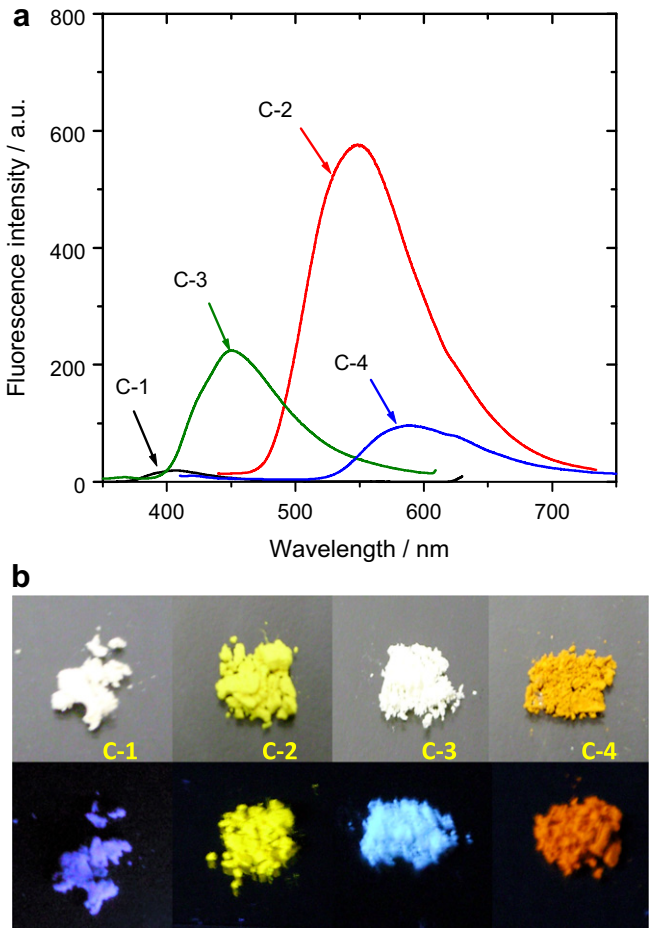

Fig. 4. (a) Emission spectra of compounds **C-1**, **C-2**, **C-3** and **C-4** in solid state, λ_{ex} [**C-1**] = 300 nm, λ_{ex}[**C-2**] = 380 nm, λ_{ex} [**C-3**] = 315 nm, λ_{ex} [**C-4**] = 390 nm. Note the emission intensity is quasi-quantitative. (b) Photographs of compounds **C-1**, **C-2**, **C-3** and **C-4** in solid state under ambient light and UV light (hand-hold UV lamp, 365 nm), 20 °C.

shift [10,17]. The properties similar to **C-2** and **C-3** are rarely reported.

The emission of **C-4** is highly sensitive to the polarity of the solvents. For example, **C-4** is emissive in toluene, but the emission is completely quenched in other common organic solvents. We propose the emission can be quenched by the ICT effect, which is more significant in polar solvents.

3.4. Triplet excited state of the coumarin derivative

For **C-3** with the bromine atom the triplet excited state of this dye may probably be populated upon photoexcitation, due to the heavy atom effect of the bromine atom. Population of the triplet excited state of the organic chromophores is significant because these organic chromophores can be used as triplet photosensitizers to replace the noble metal complex triplet photosensitizers, such as those Pt(II), Ir(III) or Ru(II) complexes, in photocatalysis or triplet–triplet annihilation based upconversions [18–26].

In order to study the possible population of the triplet excited state of **C-3**, nanosecond time-resolved transient difference absorption spectroscopy was studied (Fig. 6). Upon pulsed 355 nm laser excitation, the transient difference absorption spectra of **C-3** were recorded (Fig. 6). A significant bleaching at 320 nm was observed, which is due to the depletion of the ground state of **C-3**. The bleaching is at the steady-state UV–Vis absorption band of **C-3** (Fig. 1). Furthermore, a positive transient absorption band at 439 nm was observed. The lifetime of the transient species by monitoring the decay kinetics at 320 nm was determined as 21.3 μs. The transient can be quenched in aerated solution (τ_T decreased to 0.26 μs. See the Electronic Supplementary Information), thus the transient is due to the triplet excited state of the dye upon photoexcitation [27]. For other coumarin derivatives described herein, no such transients were observed.

In order to study the triplet state character of **C-3** from a theoretical perspective, the spin density was studied (Fig. 7) [5,24,25,28–34]. The spin density surface (based on the optimized triplet state geometry) is spread over the whole molecular framework and the bromine atom is involved in the spin density surface. This is a reasonable result since the ISC requires significant involvement of the heavy atom [24]. Otherwise the ISC will be weak [35–38].

3.5. DFT calculations: rationalize the absorption/emission spectra and the large stokes shift

DFT calculations have attracted much attention for the study of fluorophores and fluorescent molecular probes [39–47]. Previously

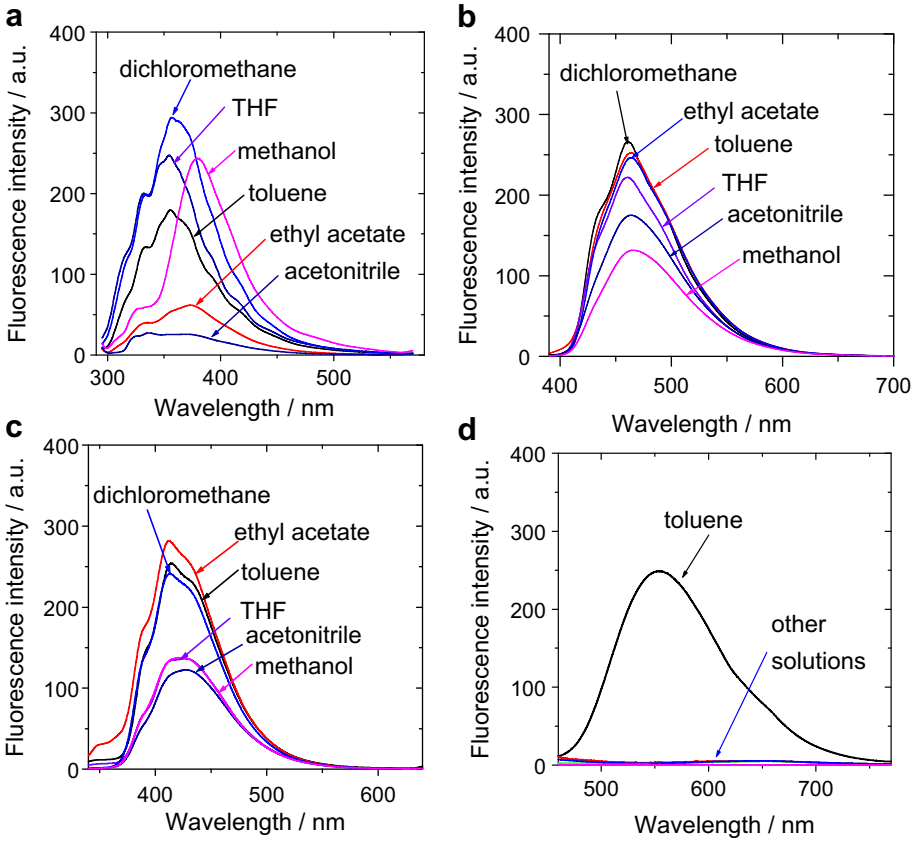

Fig. 5. Emission spectra of **C-1**, **C-2**, **C-3** and **C-4** in different solvents. (a) **C-1**, λ_{ex} = 300 nm, (b) **C-2**, λ_{ex} = 380 nm; (c) **C-3**, λ_{ex} = 315 nm; (d) **C-4**, λ_{ex} = 390 nm $c = 1.0 \times 10^{-5}$ mol dm^{-3}, 20 °C.

we used DFT calculations in the study of fluorescent thiol probes [40,46,47], and boronic acid probes [39,41,48]. We proposed to use the concept of "electronic state" rather than the conventional approximation of "molecular orbital", to study the photophysical properties, such as the fluorescence OFF–ON switching effect of the molecular probes [40,46,47]. We also proposed to use the concept of "dark excited state" and "emissive excited state" to rationalize the fluorescence transduction of the molecular probes [40,46,47]. Previously DFT calculations have also been used for study of the photophysical properties of coumarin [49].

Herein we will use DFT calculation to rationalize the photophysical properties of the new coumarin derivatives, such as the absorption/emission, and most importantly, the origin of the large Stokes shifts (Fig. 2). Experiments have shown that the Stokes shifts of **C-2**, **C-3** and **C-4** are much larger than that of the model compound **C-1**. By study the Jablonski diagram of the absorption/

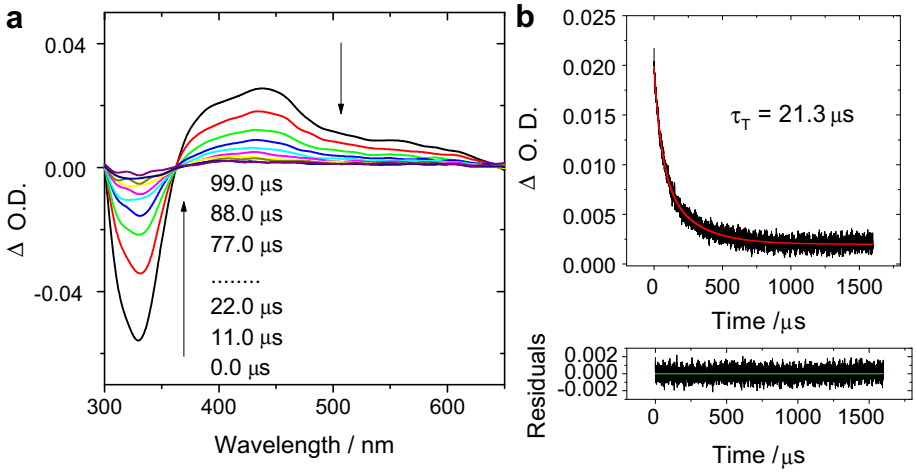

Fig. 6. (a) Nanosecond time-resolved transient difference absorption spectra and (b) decay trace of **C-3** at 320 nm after pulsed laser excitation (λ_{ex} = 355 nm). 1.5×10^{-5} mol dm^{-3} in deaerated toluene, 20 °C.

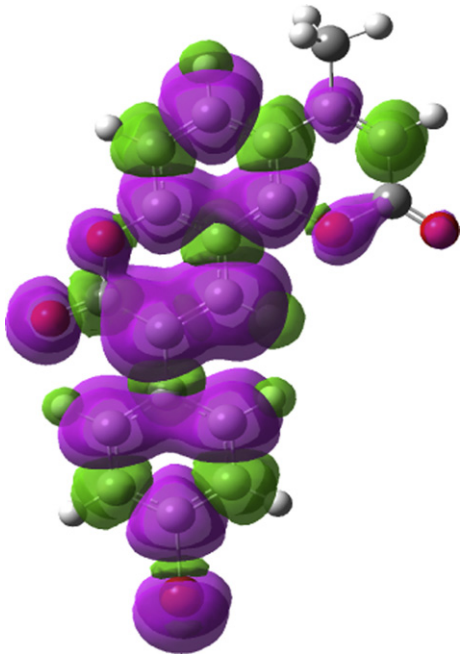

Fig. 7. The spin density surfaces of **C-3** at the triplet state. Calculated at B3LYP/6-31G(d) level with Gaussian 09W.

emission processes of chromophores [10,17], one would realize that the most probable origin of Stokes shift is the molecular geometry relaxation of the fluorophore upon photoexcitation. We propose this rule may be applicable for the present dyes, thus the geometry of **C-2**, **C-3** and **C-4** at ground state and the lowest-lying singlet excited state (S_1 state, which is responsible for the fluorescence in most cases, Kasha's rule), were optimized (Fig. 8).

For **C-2,** the most prominent feature of the ground state (S_0) geometry is the non-planar geometry of the benzothiazole against the fused coumarin moieties. A C–C single bond is the connection of the two units, thus the rotation about this bond is possible. At S_0 state, the dihedral angle between the two units is 30°. At S_1 excited state, however, the dihedral angle is 0°. That is, the fused coumarin unit and the benzothiazole unit are coplanar in the S_1 state. Similar geometry changes were found for **C-3** and **C-4** (Fig. 8).

The remarkable geometry difference between the ground state and the first singlet excited state (S_1 state) may be responsible for the large Stokes shift of the dyes **C-2**, **C-3** and **C-4** [10,17]. For the model compound **C-1**, however, we propose that the geometry relaxation is much smaller because no such dihedral angle exists.

The vertical excitation and the emission of the compounds were studied by the TDDFT calculations, based on the ground state (S_0) geometry and the optimized S_1 state geometry.

Firstly the excitation of **C-1** was calculated. The calculated absorption is at 297 nm (Fig. 9 and Table 2), which is close the experimental results (λ_{ex} = 300 nm, Fig. 1). The HOMO→LUMO transition is involved in the excitation. Both orbitals are localized on the coumarin framework. The emission of **C-1** was also calculated based on the optimized S_1 state geometry. The calculated emission wavelength is 329 nm, which is in good agreement with the experimental results of 356 nm (Fig. 2).

Small oscillator strength was found for both the absorption and the emissive transitions of **C-1** (Table 2), which indicate weak absorption and non-efficient emission. This is in line with the small

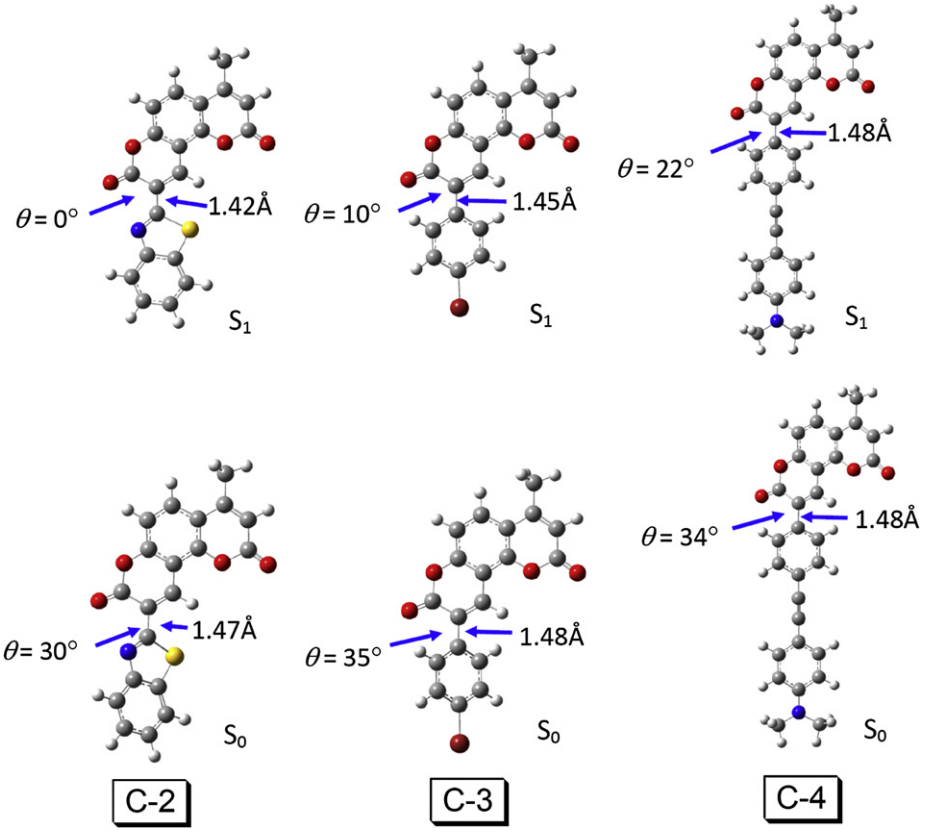

Fig. 8. Geometry of the coumarins **C-2**, **C-3** and **C-4** at the ground state (S_0) and the singlet excited state (S_1). Toluene was used as solvent in the calculation. Calculated at B3LYP/6-31g(d) level with Gaussian 09W.

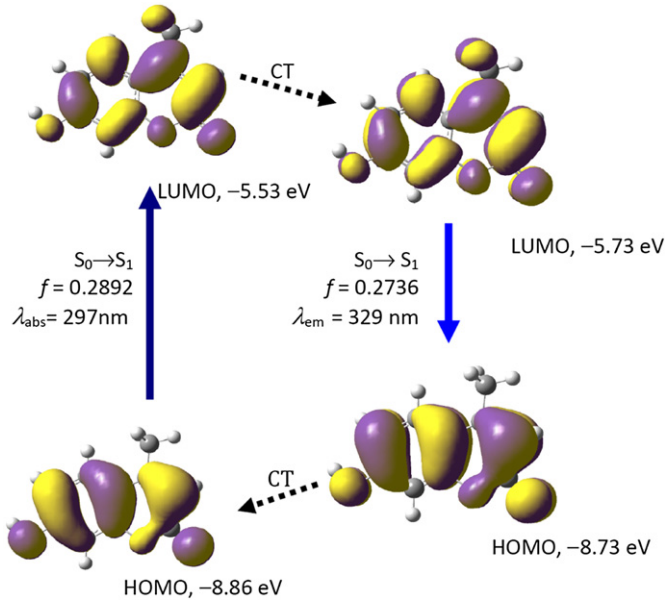

Fig. 9. The frontier MOs involved in the vertical excitation and the emission of coumarin **C-1**. CT stands for conformation transformation. Calculated with TDDFT method based on the optimized ground state (S_0) and the lowest-lying singlet excited state (S_1) geometry. Toluene was used as solvent in the calculations. Calculated at B3LYP/6-31g(d) level with Gaussian 09W.

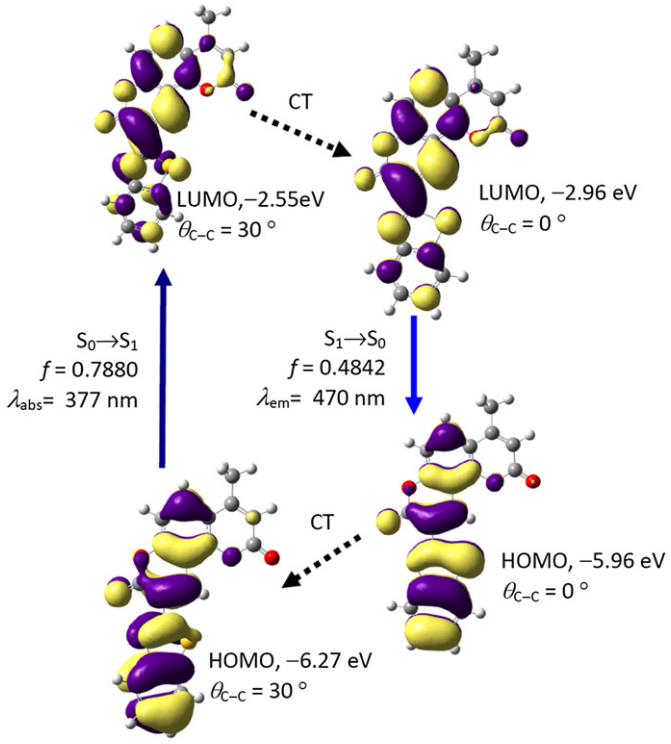

Fig. 10. The frontier MOs involved in the vertical excitation and the emission of **C-2**. CT stands for conformation transformation. Note the dihedral angle of the **C-2** at ground state is 30°, but the angle is 0° at excited state (S_1). Calculated with TDDFT based on the optimized ground state (S_0) and the S_1 state geometry. Toluene was used as solvent in the calculation. Calculated at B3LYP/6-31g(d) level with Gaussian 09W.

molar extinction coefficient and the low fluorescence quantum yield of **C-1** ($\Phi_F = 3.7\%$. Table 1).

The absorption and emission of **C-2** were also studied by the TDDFT calculations (Fig. 10 and Table 3). The benzothiazole moiety of **C-2** contributes significantly to the HOMO, whereas the LUMO is more localized on the fused coumarin moiety. The calculated excitation wavelength is 377 nm, which is in very good agreement with the experimental results of 373 nm (Fig. 1 and Table 1).

In order to study the emission of **C-2,** the geometry of the S_1 excited state was optimized (Fig. 10). The most significant difference between the ground state geometry and the S_1 state geometry is the dihedral angle between the benzothiazole moiety and the fused coumarin moiety. For the ground state (S_0 state), the dihedral angle is 30°. For the optimized S_1 state, the dihedral angle is 0°, that is, the two units are in coplanar conformation (Figs. 8 and 10).

With remarkable geometry relaxation, we observed a significant variation of the energy levels of LUMO orbital. The LUMO energy level decreased from −2.55 eV of the Franck–Condon state, to −2.96 eV of the optimized S_1 state (after geometry relaxation at the S_1 state), the stabilization is 0.41 eV. By comparison, without the significant geometry relaxation, **C-1** shows the corresponding energy level change of only 0.2 eV (Fig. 9). For **C-2**, the energy level of the HOMO at the S_1 state geometry is destabilized by 0.31 eV, compared to the HOMO at the S_0 state geometry. By comparison, **C-1** shows the corresponding de-stabilization of only 0.13 eV (Fig. 9).

Based on the results of **C-2**, it is clear that the geometry relaxation of the fluorophore upon photoexcitation (at both the S_1 state and the S_0 state) introduces large Stokes shift. Without remarkable

Table 2
Selected electronic excitation energies (eV) and corresponding oscillator strengths (*f*), main configurations and CI coefficients of the low-lying electronically excited states of **C-1**.[a]

Electronic transition	TDDFT//B3LYP/6−31G(d)			
	Energy[b]	*f*[c]	Composition[d]	CI[e]
$S_0 \rightarrow S_{1(Ex)}$	4.16 eV (297 nm)	0.2892	H → L	0.6741
			H − 1 → L	0.1233
$S_0 \rightarrow S_{2(EX)}$	4.51 eV (275 nm)	0.0228	H → L	0.1287
			H − 1 → L	0.6230
$S_1 \rightarrow S_{0(EM)}$	3.76 eV (329 nm)	0.2736	H → L	0.6760
			H − 1 → L + 1	0.1115
			H − 1 → L	0.1555
$S_2 \rightarrow S_{0(EM)}$	4.19 eV (295 nm)	0.0522	H → L	0.1461
			H − 1 → L	0.6503

[a] Excitations were calculated by TDDFT//B3LYP/6-31G(d), based on the optimized ground state geometries. The emissions were calculated based on the optimized excited state geometries. Toluene was used as solvent in the calculations.
[b] Only the low-lying excited state and some major allowed transitions were presented.
[c] Oscillator strength.
[d] Only the main configuration interaction (CI) coefficients >0.1 are presented. H stands for HOMO and L stands for LUMO.
[e] CI coefficients are in absolute values.

Table 3
Selected electronic excitation energies (eV), corresponding oscillator strengths (*f*), main configurations and CI coefficients of the low-lying electronically excited states of **C-2**. [a]

Electronic transition	TDDFT//B3LYP/6−31G(d)			
	Energy (eV)	f	Composition	CI
$S_0 \rightarrow S_{1(EX)}$	3.29 eV (377 nm)	0.7880	H → L	0.6903
			H−1 → L	0.1206
$S_0 \rightarrow S_{2(EX)}$	3.43 eV (361 nm)	0.0411	H→L	0.1219
			H − 1 → L	0.6888
$S_1 \rightarrow S_{0(EM)}$	2.63 eV (470 nm)	0.7185	H → L	0.6903
			H − 1 → L	0.1465
$S_2 \rightarrow S_{0(EM)}$	3.05 eV (407 nm)	0.2602	H → L	0.1464
			H − 1 → L	0.6863

[a] For the meaning of the table contents, please refer to Table 2.

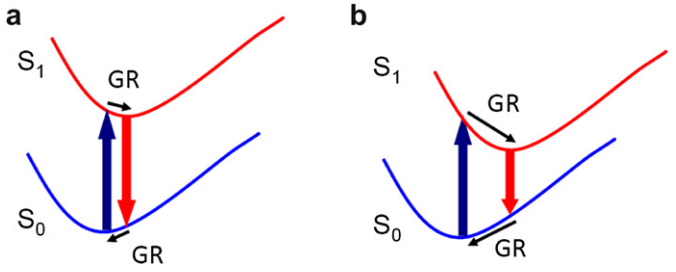

Fig. 11. Simplified Jablonski diagram for the origin of Stokes shifts of the coumarin dyes. (a) Small geometry relaxation upon photoexcitation produces small Stokes shift, which is applicable to **C-1**. (b) Large geometry relaxation upon photoexcitation leads to large Stokes shift, which is applicable to **C-2**, **C-3** and **C-4**. GR stands for geometry relaxation.

Table 4
Selected electronic excitation energies (eV) and corresponding oscillator strengths (*f*), main configurations and CI coefficients of the low-lying electronically excited states of **C-3**.[a]

Electronic transition	TDDFT//B3LYP/6−31G(d)			
	Energy (eV)	*f*	Composition	CI
$S_0 \rightarrow S_{1(EX)}$	3.49 eV (355 nm)	0.6657	H → L	0.6856
			H − 1 → L	0.1494
$S_0 \rightarrow S_{2(EX)}$	3.66 eV (338 nm)	0.0712	H → L	0.1511
			H → L + 1	0.3586
			H − 1 → L	0.5681
$S_1 \rightarrow S_{0(EM)}$	2.87eV (432 nm)	0.8389	H → L	0.7032
$S_2 \rightarrow S_{0(EM)}$	3.31 eV (374 nm)	0.0284	H → L + 1	0.4643
			H − 1 → L	0.5181

[a] For the meaning of the table contents, please refer to Table 2.

geometry relaxation at the S_1 state, small Stokes shift will be observed, which is applicable to **C-1**.

The difference of the Stokes shift of **C-1** and **C-2** can be explained by Fig. 11. Small geometry relaxation of the fluorophore upon photoexcitation will lead to small Stokes shift (Fig. 11a), which is applicable to **C-1**. Conversely, large geometry relaxation upon photoexcitation will produce large Stokes shift. This is applicable for **C-2**.

The above theoretical calculations on the photophysical properties were further confirmed by study of **C-3** (Fig. 12 and Table 4). The calculated excitation energy of **C-3** is 355 nm, which is close to the experimental results of 327 nm (Fig. 1 and Table 1). Geometry relaxation was also observed for **C-3** at the S_1 state (the dihedral angle between the benzenethiazole moiety and the fused coumarin unit changed from 35° to 10°) (Fig. 8). The calculated emission wavelength is 432 nm, which is close to the experimental result of 410 nm (Fig. 2 and Table 1).

Based on the frontier orbitals involved in the absorption and emission transitions (Table 4), we propose that the coumarin unit is more involved in the HOMO and LUMO orbitals. Furthermore, the phenyl moiety is involved in the orbitals, thus we propose the photophysical properties of the fused coumarin chromophore can be tuned by using different substituents at the phenyl position. The results of **C-4** proved this postulation.

The excitation and emission of **C-4** were studied with similar methods (Fig. 13 and Table 5). We found that the HOMO and LUMO orbitals of **C-4** are more localized than the other derivatives studied

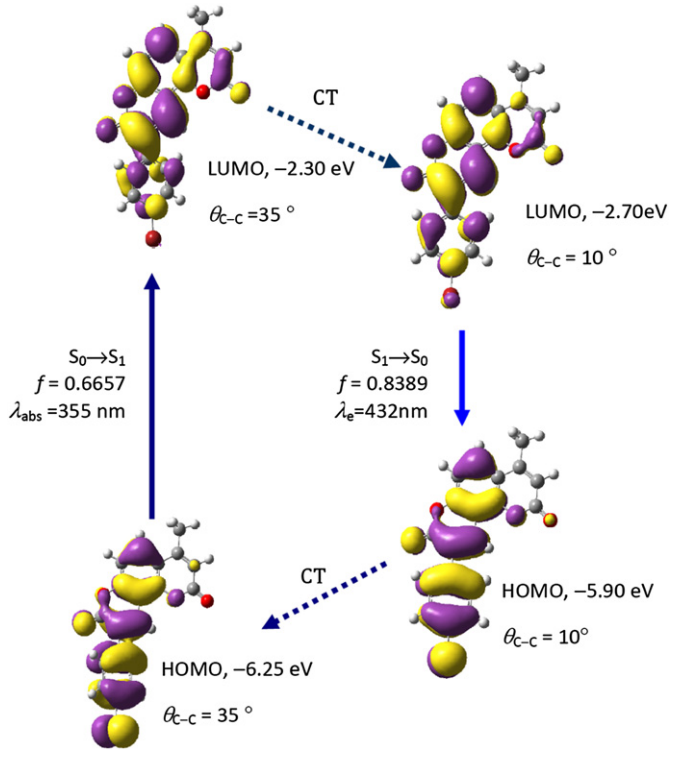

Fig. 12. The frontier MOs involved in the vertical excitation and the emission of **C-3**. CT stands for conformation transformation. Note the dihedral angle of the **C-3** at ground state is 35°, but the angle is 10° at excited state (S_1). Calculated with TDDFT based on the optimized ground state (S_0) and the lowest-lying singlet excited state (S_1) geometry. Toluene was used as solvent in the calculation. Calculated at B3LYP/6-31g(d) level with Gaussian 09W.

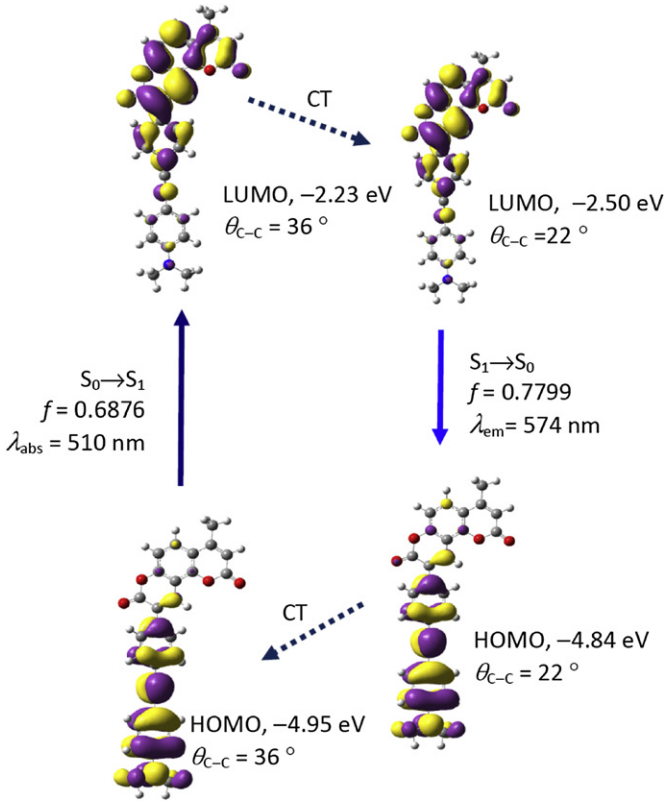

Fig. 13. The frontier MOs involved in the vertical excitation and the emission of **C-4**. CT stands for conformation transformation. Note the dihedral angle of the fused coumarin and the phenyl moiety at ground state is 36°, but the angle is 22° at excited state (S_1). Calculated with TDDFT based on the optimized ground state (S_0) and the lowest-lying singlet excited state (S_1) geometry. Toluene was used as solvent in the calculation. Calculated at B3LYP/6-31g(d) level with Gaussian 09W.

Table 5
Selected electronic excitation energies (eV) and corresponding oscillator strengths (*f*). Main configurations and CI coefficients of the low-lying electronically excited states of **C-4**. [a]

Electronic transition	TDDFT//B3LYP/6–31G(d)			
	Energy	*f*	Composition	CI
$S_0 \rightarrow S_{1(EX)}$	2.43 eV (510 nm)	0.6876	H → L	0.7031
$S_0 \rightarrow S_{2(EX)}$	2.85 eV (434 nm)	0.0313	H → L + 1	0.7025
$S_0 \rightarrow S_{3(EX)}$	3.46 eV (358 nm)	1.1128	H − 1 → L	0.5871
			H → L+2	0.3696
$S_1 \rightarrow S_{0(EM)}$	2.16 eV (574 nm)	0.8036	H → L	0.7050
$S_2 \rightarrow S_{0(EM)}$	2.70 eV (459 nm)	0.0150	H → L + 1	0.7029

[a] For the meaning of the table contents, please refer to Table 2.

herein. For example, at both the S_0 state geometry and the S_1 state geometry, both HOMO are localized on the acetylide phenyl moieties. For the LUMO, however, the orbitals are more localized on the fused coumarin moiety. Thus the ICT character of **C-4** is more significant than the other dyes. The calculated excitation energy is 2.43 eV (510 nm, Fig. 13), which is much smaller than the experimental results of 3.19 eV (389 nm, Fig. 1 and Table 1). This is within expectation because DFT method usually gives under-estimated excitation energy for the charge transfer excitations [38,50]. The calculated emission wavelength is 574 nm (Fig. 13), which is close to the experimental result of 555 nm (Fig. 2 and Table 1).

Based on the MOs of **C-4** (Fig. 13), the intramolecular charge transfer of **C-4** is significant, which is probably responsible for the emission properties of **C-4**, such as the sensitivity to the polarity of the solvents.

Our DFT and TDDFT calculations on the dyes **C-1**–**C-4** demonstrated that the large Stokes shift of **C-2**, **C-3** and **C-4** are due to the significant geometry relaxation of the dyes upon photoexcitation. This is in agreement with the Jablonski diagram of the fluorescence process [10,17]. Furthermore, the UV–Vis absorption and the fluorescence emission of the dyes were predicted by the TDDFT calculations. The molecular orbitals demonstrated the significant ICT character of **C-4**, which is in agreement with the experimental results. The calculation results are useful for rationale design of new fluorophores.

4. Conclusions

New fluorophores with novel *fused coumarin* framework were prepared (**C-2**, **C-3** and **C-4**). These fused coumarin dyes show red-shifted and enhanced absorption and emissions compared to the model compound (7-hydroxycoumarin, **C-1**). For example, **C-2** (with benzenthiazole functionalization) shows absorption at 373 nm ($\varepsilon = 9140\ M^{-1}\ cm^{-1}$) and emission at 461 nm. **C-4**, with a 4-dimethylaminophenylacetylide substituent, shows absorption at 389 nm ($\varepsilon = 14{,}300\ M^{-1}\ cm^{-1}$), compared to the model coumarin **C-1**. Furthermore, the fluorescence quantum yields of the fused coumarins ($\Phi_F = 32.3\%$ for **C-4**) are up to ca. 9-fold of the model coumarin ($\Phi_F = 3.7\%$ for **C-1**). Most importantly, the Stokes shifts of the new fused coumarin dyes (84 nm–166 nm) are much larger than the model coumarin (56 nm). The new functionalized fused coumarin dyes show solvent polarity-dependent emission intensity, but the emission wavelength does not change in different solvents. The photophysical properties of the new dyes were fully rationalized by DFT/TDDFT calculations. The TDDFT calculations show that the new dyes undergo significant geometry relaxation upon photoexcitation, which is responsible for the large Stokes shifts. Population of the triplet excited state at room temperature was observed for the bromo-functionalized fused coumarin derivative. Our complementary experimental and theoretical study on the new dyes with novel fused coumarin structure is useful for design of new fluorophores that show predetermined photophysical properties, especially large Stokes shift.

Acknowledgments

We thank the NSFC (20972024 and 21073028), the Fundamental Research Funds for the Central Universities (DUT10ZD212), the Royal Society (UK) and NSFC (China-UK Cost-Share Science Networks, 21011130154), Ministry of Education (NCET-08-0077) and State Key Laboratory of Fine Chemicals (KF0802) for financial support.

Appendix A. Supplementary information

Supplementary data related to this article can be found online at doi:10.1016/j.dyepig.2012.04.024

References

[1] Reymond JL, Fluxà VS, Maillard N. Enzyme assays. Chem Commun; 2009:34–46.
[2] (a) Maton L, Taziaux D, Soumillion JP, Jiwan JL H. About the use of an amide group as a linker in fluoroionophores: competition between linker and ionophore acting as chelating groups. J Mater Chem 2005;15:2928–37;
(b) Botek E, d'Antuono P, Jacques A, Carion R, Champagne B, Maton L, et al. Theoretical and experimental investigation of the structural and spectroscopic properties of coumarin 343 fluoroionophores. Phys Chem Chem Phys 2010; 12:14172–87.
[3] Xie L, Chen Y, Wu W, Guo H, Zhao J, Yu X. Fluorescent coumarin derivatives with large stokes shift, dual emission and solid state luminescent properties: an experimental and theoretical study. Dyes Pigm 2012;92:1361–9.
[4] (a) Tyson DS, Castellano FN. Light–harvesting arrays with coumarin donors and MLCT acceptors. Inorg Chem 1999;38:4382–3;
(b) Frederich N, Nysten B, Muls B, Hofkens J, Habib-Jiwan JL, Jonas AM. Nanopatterned layers of a grafted coumarinic chromophore. Photochem Photobiol Sci 2008;7:460–6.
[5] Sun J, Wu W, Guo H, Zhao J. Visible–light harvesting with cyclometalated iridium(III) complexes having long–lived 3IL excited states and their application in triplet–triplet–annihilation based upconversion. Eur J Inorg Chem; 2011:3165–73.
[6] Choi MG, Kim YH, Namgoong JE, Chang SK. Hg^{2+}-selective chromogenic and fluorogenic chemodosimeter based on thiocoumarins. Chem Commun; 2009:3560–2.
[7] Lin W, Yuan L, Cao Z, Feng Y, Long L. A sensitive and selective fluorescent thiol probe in water based on the conjugate 1,4–addition of thiols to α,β–unsaturated ketones. Chem Eur J 2009;15:5096–103.
[8] Lee KS, Kim TK, Lee JH, Kim HJ, Hong JI. Fluoresc– ence turn–on probe for homocysteine and cysteine in water. Chem Commun; 2008:6173–5.
[9] Lin W, Long L, Tan W. A highly sensitive fluorescent probe for detection of benzenethiols in environmental samples. Chem Commun 2010;46:1503–5.
[10] Lakowicz JR. Principles of fluorescence spectroscopy. 3rd ed. Berlin Heidelberg: Springer-Verlag; 2006.
[11] Schiedel MS, Briehn CA, Bauerle P. Single-compound libr – aries of organic materials: parallel synthesis and screening of fluorescent dyes. Angew Chem Int Ed 2001;40:4677–80.
[12] (a) Elangovan A, Lin JH, Yang SW, Hsu HY, Ho TI. Synthesis and electro-generated chemiluminescence of donor–substituted phenyl-ethynylcoumarins. J Org Chem 2004;69:8086–92;
(b) Chao RY, Ding MF, Chen JY, Lee CC, Lin ST. Preparation and characterization of substituted 3-benzothiazol-2-ylcoumarins. J Chin Chem Soc 2010;57: 213–21.
[13] Frisch MJ, Trucks GW, Schlegel HB, Scuseria GE, Robb MA, Cheeseman JR, et al. Gaussian 09 (Revision A.1). Wallingford CT: Gaussian, Inc; 2009.
[14] Uchiyama S, Takehira K, Yoshihara T, Tobita S, Ohwada T. Environment–sensitive fluorophore emitting in protic environments. Org Lett 2006; 8:5869–72.
[15] Kulkarni A, Patil SA, Badami PS. Synthesis, characterization, DNA cleavage and in vitro antimicrobial studies of La(III), Th(IV) and VO(IV) complexes with schiff bases of coumarin derivatives. Eur J.Med Chem 2009;44:2904–12.
[16] Lu H, Xiong LQ, Liu HZ, Yu MX, Shen Z, Li FY, et al. A highly selective and sensitive fluorescent turn–on sensor for Hg^{2+} and its application in live cell imaging. Org Biomol Chem 2009;7:2554–8.
[17] Turro NJ, Ramamurthy V, Scaiano JC. Principles of molecular photochemistry; an introduction. Sausalito; CA: University Science Books; 2009.
[18] Celli JP, Spring BQ, Rizvi I, Evans CL, Samkoe KS, Verma S, et al. Imaging and photodynamic therapy: mechanisms, monitoring and optimization. Chem Rev 2010;110:2795–838.

[19] P. Elmes RB, Erby M, Cloonan SM, Quinn SJ, Williams DC, Gunnlaugsson T. Quaternarized pdppz: synthesis, DNA-binding and biological studies of a novel dppz derivative that causes cellular death upon light irradiation. Chem Commun 2011;47:686–8.
[20] Singh–Rachford TN, Castellano FN. Photon upconversion based on sensitized triplet–triplet annihilation. Coord Chem Rev 2010;254:2560–73.
[21] Zhao J, Ji S, Guo H. Triplet–triplet annihilation based upconversion: from triplet sensitizers and triplet acceptors to upconversion quantum yields. RSC Adv 2011;1:937–50.
[22] Chen HC, Hung CY, Wang KH, Chen HL, Fann WS, Chien FC, et al. White–light emission from an upconverted emission with an organic triplet sensitizer. Chem Commun; 2009:4064–6.
[23] Singh–Rachford TN, Castellano FN. Low power visible–to–UV upconversion. J Phys Chem A 2009;113:5912–7.
[24] Wu W, Guo H, Wu W, Ji S, Zhao J. Organic triplet sensitizer library derived from a single chromophore (BODIPY) with long-lived triplet excited state for triplet-triplet annihilation based upconversion. J Org Chem 2011;76:7056–64.
[25] Ji S, Guo H, Wu W, Wu W, Zhao J. Ruthenium(II)polyimine–coumarin dyad with nonemissive ^{3}IL excited state as sensitizer for triple–triplet annihilation based upconversion. Angew Chem Int Ed 2011;50:8283–6.
[26] Ji S, Wu W, Wu W, Guo H, Zhao J. Ruthenium(II) polyimine complexes with a long-lived ^{3}IL excited state or a ^{3}MLCT/^{3}IL equilibrium: efficient triplet sensitizers for low-power upconversion. Angew Chem Int Ed 2011;50:1626–9.
[27] Iijima T, Momotake A, Shinohara Y, Sato T, Nishimura Y, Arai T. Excited–state intramolecular proton transfer of naphthalene-fused 2-(2-Hydroxyaryl) benzazole Family. J Phys Chem A 2010;114:1603–9.
[28] Hanson K, Tamayo A, Diev VV, Whited MT, Djurovich PI, Thompson ME. Efficient dipyrrin–centered phosphorescence at room temperature from bis–cyclometalated Iridium(III) dipyrrinato complexes. Inorg Chem 2010;49:6077–84.
[29] Liu Y, Guo H, Zhao J. Ratiometric luminescent molecular oxygen sensors based on uni-luminophores of *C^N* Pt(II)(acac) complexes that show intense visible-light absorption and balanced fluorescence phosphorescence dual emission. Chem Commun 2011;47:11471–3.
[30] Wu W, Sun J, Ji S, Wu W, Zhao J, Guo H. Tuning the emissive triplet excited states of platinum(II) schiff base complexes with pyrene and application for luminescent oxygen sensing and triplet–triplet–annihilation based upconversions. Dalton Trans 2011;40:11550–61.
[31] Huang L, Zeng L, Guo H, Wu W, Wu W, Ji S, et al. Room-temperature long-lived 3IL excited state of rhodamine in an *N^N* Pt^{II} bis(acetylide) complex with Intense visible-light absorption. Eur J Inorg Chem; 2011:4527–33.
[32] Liu Y, Wu W, Zhao J, Zhang X, Guo H. Accessing the long-lived near-IR-emissive triplet excited state in naphthalenediimide with light–harvesting diimine platinum(II) bisacetylide complex and its application for upconversion. Dalton Trans 2011;40:9085–9.
[33] Sun H, Guo H, Wu W, Liu X, Zhao J. Coumarin phos–phorescence observed with *N^N* Pt(II) bisacetylide complex and its applications for luminescent oxygen sensing and triplet–triplet–annihilation based upconversion. Dalton Trans 2011;40:7834–41.
[34] Wu W, Wu W, Ji S, Guo H, Zhao J. Accessing the long-lived emissive ^{3}IL triplet excited states of coumarin fluorophores by direct cyclo − metallation and its application for oxygen sensing and upconversion. Dalton Trans 2011;40:5953–63.
[35] Tahtaoui C, Thomas C, Rohmer F, Klotz P, Duportail G, Mély Y, et al. Convenient method to access new 4,4-dialkoxy and 4,4-diaryloxy–diaza–*s*–indacene dyes: synthesis and spectroscopic evaluation. J Org Chem 2007;72:269–72.
[36] Azov VA, Schlegel A, Diederich F. Functionalized calix[4]resorcinarene cavitands. Versatile platforms for the modular construction of extended molecular switches. Bull Chem Soc Jpn 2006;79:1926–40.
[37] Singh-Rachford TN, Haefele A, Ziessel R, Castellano FN. Boron dipyrromethene chromophores: next generation triplet acceptors/annihilators for low power upconversion schemes. J Am Chem Soc 2008;130:16164–5.
[38] Kowalczyk T, Lin ZL, Voorhis TV. Fluorescence quenching by photoinduced electron transfer in the Zn^{2+} sensor zinpyr-1: a computational investigation. J Phys Chem A 2010;114:10427–34.
[39] Han F, Chi L, Liang X, Ji S, Liu S, Zhou F, et al. 3,6-Disubstituted carbazole-based bisboronic acids with unusual fluorescence transduction as enantioselective fluorescent chemosensors for tartaric acid. J Org Chem 2009;74:1333–6.
[40] Ji S, Yang J, Yang Q, Liu S, Chen M, Zhao J. Tuning the intramolecular charge transfer of alkynylpyrenes: effect on photophysical properties and its application in design of OFF–ON fluorescent thiol probes. J Org Chem 2009;74:4855–65.
[41] Zhang X, Chi L, Ji S, Wu Y, Song P, Han K, et al. Rational design of d-PeT phenylethynylated-carbazole monoboronic acid fluorescent sensors for the selective detection of α-hydroxyl carboxylic acids and monosaccharides. J Am Chem Soc 2009;131:17452–63.
[42] Larkin JD, Fossey JS, James TD, Brooks BR, Bock CW A. Computational investigation of the nitrogen–boron Interaction in o-(*N*,*N*-dialkylaminomethyl) arylboronate systems. J Phys Chem A 2010;114:12531–9.
[43] Zhao G, Liu J, Zhou L, Han K. Site-selective photoinduced electron transfer from alcoholic solvents to the chromophore facilitated by hydrogen bonding: a new fluorescence quenching mechanism. J Phys Chem B 2007;111:8940–5.
[44] Gabe Y, Urano Y, Kikuchi K, Kojima H, Nagano T. Highly sensitive fluorescence probes for nitric oxide based on boron dipyrromethene chromophore rational design of potentially useful bioimaging fluorescence probe. J Am Chem Soc 2004;126:3357–67.
[45] Yuan Z, Xiao Y, Li Z, Qian X. Efficient synthesis of regioisomerically pure bis(trifluoromethyl)-substituted 3,4,9,10-perylene tetracarboxylic bis–(benzimidazole). Org Lett 2009;11:2808–11.
[46] Guo H, Jing Y, Yuan X, Ji S, Zhao J, Li X, et al. Hightly selective fluorescent OFF–ON thiol probes based on dyads of BODIPY and potent intramolecular electron sink 2,4–dinitrobenzenesulfonyl subunits. Org Biomol Chem 2011;9:3844–53.
[47] Shao J, Guo H, Ji S, Zhao J. Styryl-BODIPY based red–emitting fluorescent OFF–ON molecular probe for specific detection of cysteine. Biosens Bioelectron 2011;26:3012–7.
[48] Zhang X, Wu Y, Ji S, Guo H, Song P, Han K, et al. Effect of the electron donor/acceptor orientation on the fluorescence transduction efficiency of the d-PET effect of carbazole based fluorescent boronic acid sensors. J Org Chem 2010;75:2578–88.
[49] (a) Cave RJ, Burke K, Castner Jr EW. Theoretical investigation of the ground and excited states of coumarin 151 and coumarin 120. J Phys Chem A 2002;106:9294–305;
(b) Kurashige Y, Nakajima T, Kurashige S, Hirao K, Nishikitani Y. Theoretical investigation of the excited states of coumarin dyes for dye-sensitized solar cells. J Phys Chem A 2007;111:5544–8.
[50] Dreuw A, Weisman JL, Head-Gordon M. Long-range charge-transfer excited states in time-dependent density functional theory require non-local exchange. J Chem Phys 2003;119:2943–6.